Cellular & Molecular Biology Letters

RESEARCH ARTICLE Open Access

DNA dioxygenase TET2 deficiency aggravates sepsis-induced acute lung injury by targeting ITGA10 via the PI3K/AKT signaling pathway

Hongxue Fu[1], Bin Gao[1], Xin Zhou[1], Yingting Hao[1], Chang Liu[1], Ailin Lan[1], Jingyi Tang[2,3*] and Fachun Zhou[1*]

*Correspondence:
jingyitang@cqut.edu.cn;
cyzfc1966@126.com

[1] Department of Critical Care Medicine, The First Affiliated Hospital of Chongqing Medical University, Chongqing 400016, China
[2] School of Pharmacy and Bioengineering, Chongqing University of Technology, Chongqing 400054, China
[3] Chongqing Key Laboratory of Translational Research for Cancer Metastasis and Individualized Treatment, Chongqing University Cancer Hospital, Chongqing 400030, China

Abstract

Background: Sepsis-induced acute lung injury (ALI) is a clinical condition with high morbidity and mortality, and impaired endothelial function is the main pathological characteristic. As a member of DNA demethylases, ten-eleven translocation protein 2 (TET2) is involved in a variety of biological processes. However, the role of *TET2* in endothelial dysfunction of sepsis-induced ALI remains unclear.

Methods: We used cecal ligation and puncture (CLP) to establish a sepsis-induced acute lung injury mouse model and screened out Tet2 from TET family proteins. The results suggested that Tet2 was obviously declined. We used lipopolysaccharide (LPS) to stimulate human pulmonary microvascular endothelial cells (HPMECs) as an in vitro model, and we found the expression of TET2 was also decreased. Then we used small interfering RNAs and adenovirus to knockdown or overexpress *TET2* to investigate the effect of *TET2* on the function of HPMECs. The changes in sepsis-induced ALI symptoms were also analyzed in *Tet2*-deficient mice generated by adeno-associated virus 6 (AAV6). Next, RNA sequencing and KEGG analysis were used to find the *TET2*-regulated downstream target genes and signaling pathways under LPS stimulation. Finally, the rescue experiments were performed to analyze the role of target genes and signaling pathways modulated by *TET2* in LPS-treated HPMECs.

Results: TET2 and 5-hmC levels were significantly decreased in both in vitro and in vivo models of sepsis-induced ALI. *TET2* knockdown exacerbated the dysfunction and apoptosis of HPMECs induced by LPS. Conversely, *TET2* overexpression significantly alleviated these dysfunctions and reduced apoptosis. Meanwhile, the lung injury of *Tet2*-deficient mice was aggravated by increased inflammation and apoptosis. RNA sequencing and subsequent experiments showed that *TET2* overexpression could increase the expression of *Integrin α10* (*ITGA10*) by reducing the methylation level of *ITGA10* promoter. This, in turn, activated the PI3K-AKT signaling pathway. Knocking down *ITGA10* weakened the beneficial effects of *TET2* overexpression in LPS-stimulated endothelial cells.

Conclusions: In our study, we demonstrated that *TET2* deficiency aggravates endothelial cell dysfunction and promotes acute lung injury by targeting *ITGA10*

via the PI3K-AKT pathway. These findings indicate that *TET2* may be a promising therapeutic target for treating sepsis-induced ALI.

Highlights

1. The expression of TET2 and 5-hmC was significantly decreased in both in vivo and in vitro models of sepsis-induced acute lung injury.
2. *Tet2* deficiency aggravates acute lung injury in septic mice and exacerbates dysfunction of human pulmonary microvascular endothelial cells induced by LPS.
3. *TET2* may play a key role in sepsis-induced acute lung injury by regulating *ITGA10*/PI3K/AKT pathway.

Keywords: *TET2*, 5-hmC, Endothelial cell dysfunction, *ITGA10*, Sepsis-induced acute lung injury

Introduction

Sepsis is a severe, life-threatening condition characterized by systemic organ dysfunction and a high mortality rate, resulting from various infections and eliciting a systemic inflammatory response [1, 2]. Among the organs affected by sepsis, the lungs are commonly involved, with sepsis-induced acute lung injury (ALI) being one of the earliest and most severe complications. This condition can further progress to acute respiratory distress syndrome (ARDS) and even lead to respiratory failure [3]. The dysfunction of vascular endothelial plays a pivotal role in sepsis-induced ALI, encompassing pulmonary vascular endothelial impairment, transport dysfunction, alterations in vascular tension, amplified inflammatory response, and cascade unregulated coagulation response [4, 5]. Human pulmonary microvascular endothelial cells (HPMECs) are key effector cells in sepsis-induced ALI. The excessive release of inflammatory mediators and chemokines inhibit cell viability and proliferation, and promote apoptosis of cells, resulting in HPMEC damage and increased pulmonary vascular permeability, thereby aggravating lung pathological injury [6, 7]. However, the pathophysiological mechanism of sepsis remains unclear. Recently, numerous reports have demonstrated that epigenetic modification is associated with critical stages of sepsis, including host–pathogen interaction, the acute inflammatory phase, and the immunosuppression phase, particularly leading to vascular endothelial dysfunction [8, 9].

Epigenetic modifications, such as DNA methylation, histone modifications, and non-coding RNAs, refer to DNA modifications that can regulate gene expression without changing the underlying gene sequence. Among these modifications, DNA methylation, particularly involving 5-hydroxymethylcytosine (5-hmC) and 5-methylcytosine (5-mC), has been extensively investigated [10]. It has been known that increased levels of 5-mC are generally linked to gene silencing, while 5-hmC levels are typically involved in upregulation of gene expression [11, 12]. Multiple studies have noticed that global DNA methylation levels are increased obviously in lipopolysaccharide (LPS)-induced ALI mice model compared with controls. Moreover, the use of DNA methyltransferase (Dnmt) inhibitors has been shown to reduce both serum inflammatory factors and lung injury severity in these mice [13–16], indicating the importance of DNA methylation in

regulating the progression of ALI induced by LPS. One of the instrumental protein families in DNA methylation is the ten-eleven translocation (TET) family, which consists of TET1, TET2, and TET3, serving as crucial demethylases that oxidize 5-mC to 5-hmC. Among them, *TET2* has received significant attention in latest research [17, 18]. *TET2* is recognized as an essential regulator of normal hematopoiesis, particularly in bone marrow. Mutations or loss of *TET2* result in widespread abnormal DNA hypermethylation, contributing to the development of hematological malignancies such as acute myeloid leukemia (AML), myelodysplastic syndrome (MDS), and other myeloid diseases [19]. Emerging evidence suggests that *TET2* is also crucial in regulating immune homeostasis during different stages of inflammation in various inflammatory diseases, acting through macrophages, T cells, dendritic cells (DCs), and endothelial cells [20–26]. In addition, *Tet2* deficiency can promote pulmonary diseases. For instance, during acute *Pseudomonas aeruginosa* pneumonia, one study showed that *Tet2* can enhance the junction integrity of bronchial epithelial cells [27]. In patients with pulmonary arterial hypertension (PAH), the levels of TET2 have been proved to decrease significantly, meanwhile in *Tet2*- knockout mice model, PAH developed spontaneously [28]. A similar decline in Tet2 levels has been observed in chronic obstructive pulmonary disease (COPD), where it was demonstrated that *Tet2* alleviates airway epithelial cell ferroptosis by demethylating glutathione peroxidase 4 (*Gpx4*) [29]. However, the function of *TET2* in sepsis-induced ALI has not yet been explored.

In this study, we thoroughly investigated the involvement of *Tet2* in sepsis-induced ALI and observed that *Tet2* deficiency exacerbated the pathological lung damage in a sepsis-induced ALI mouse model. Furthermore, we found that TET2 levels were decreased in LPS-stimulated HPMECs and that TET2 could relieve the dysfunction of HPMECs. Our findings suggested that *TET2* alleviates sepsis-induced ALI by targeting *ITGA10* through the PI3K-AKT signaling pathway.

Materials and methods

Cell culture and transfection

HPMECs were purchased from Sciencell (cat. no. 3000, San Diego, CA, USA) and cultured in a complete medium composed of 10% fetal bovine serum (Gibco, Paisley, UK), 89% Dulbecco's Modified Eagle Medium (DMEM; Procell, Wuhan, China), and 1% penicillin/streptomycin (Procell, Wuhan, China) at 37 °C in a humidified atmosphere containing 5% CO_2. To establish the in vitro model of sepsis-induced ALI, HPMECs were stimulated by LPS (SigmaAldrich, St. Louis, USA) at a concentration of 10 μg/mL for 12 h, following a previously described protocol [30–32]. A total of 1×10^5 cells per well were seeded into 6-well plates and allowed to incubate for 24 h. According to the manufacturer's instructions, when the density of cells reached about 50–60% with better growth, HPMECs were transfected with 150 pmol siRNAs (GenePharma, Shanghai, China) using GP-transfect-Mate (GenePharma, Shanghai, China). The siRNAs sequences are listed in Additional File 1: Supplementary Table S1. Adenovirus constructs (AD-Admax-h-*TET2*-3xflag-EGFP) for overexpression of TET2, with a multiplicity of infection of 50, were generously provided by Dr. Wanyun Zhang (Chongqing Medical University). The efficiency of siRNAs and adenovirus constructs are shown in Additional File 1: Supplementary Fig. S1 A–D.

Mouse model in vivo study

C57BL/6J mice (male, 6–8 weeks old, 18–22 g) were purchased from Chongqing Medical University Experimental Animal Center (Chongqing, China) and reared under specific pathogen-free conditions. Animals were provided unrestricted access to water and food. All animal experiments were approved by the Ethics Committee on Animal Research of Chongqing Medical University (IACUC-CQMU-2024-0706). Environmental parameters were strictly regulated, with a temperature of 22 ± 1 °C, 60% humidity, and a 12-h light/dark cycle. The *Tet2* shRNA and the control shRNA adeno-associated virus 6 were sourced from GenePharma (Shanghai, China) with titers of 2.5×10^{13} vg/mL, and mice were injected via tail vein with 2.5×10^{12} V.G/mouse. Subsequently, 4 weeks post-injection, the mice were subjected to cecal ligation and puncture to induce sepsis-induced ALI, as described previously [33]. Following surgery, mice were subcutaneously administered 0.9% saline at 37 °C for fluid resuscitation and then returned to their cages for recovery. Mice in the control group underwent a sham procedure consisting of an abdominal incision without cecal ligation and puncture.

RNA extraction and reverse transcription-quantitative polymerase chain reaction (RT-qPCR)

Total RNAs were isolated using TRIzol Reagent (R401-0, Vazyme, Nanjing, China) and then quantified with a NanoDrop 2000 spectrophotometer (Thermo Fisher, Waltham, MA, USA). A total of 1 μg RNA was used for reverse transcription into cDNA by a reverse transcription kit (RK20433, ABclonal, Wuhan, China). RT-qPCR was performed on CFX96 System (Applied Biosystems, Foster City, CA, USA) using SYBR Green Fast qPCR Mix (RK21203, ABclonal, Wuhan, China). Data were analyzed using the $2^{-\Delta\Delta Ct}$ method, and the cDNA expression levels were normalized to GAPDH. The sequences of primers are presented in Additional File 1: Supplementary Table S2.

DNA extraction and dot blot

Total DNA from cultured cells and lung tissues was extracted using DNA isolation Kit (DE-05011, Foregene, Chengdu, China). The 5-hmC dot blot assay was conducted as previously published [34]. Briefly, the isolated DNA was diluted to 100 ng/μL. Total 200 ng DNA was spotted onto Hybond-N + membranes (cat. no. G6014, Servicebio, Wuhan, China). Cross-linking of the DNA to the membranes was achieved using a Scientz03-II UV Crosslinker (Ningbo, China). The membranes were then blocked with 5% bovine serum albumin (BSA) in TBST at room temperature for 1 h and subsequently incubated with a 5-hmC antibody overnight at 4 °C. The next day, after being washed three times, the membranes were treated with horseradish peroxidase (HRP)-conjugated secondary antibody for 1 h at room temperature. Following detection with enhanced chemiluminescence (ECL) substrate, methylene blue was used to stain the membranes as a loading control. The antibody information is listed in Additional File 1: Supplementary Table S3.

Protein extraction and immunoblot analysis

Proteins from cells or lung tissues were extracted using RIPA buffer (P0013B, Beyotime, Shanghai, China), and the concentrations of protein were measured with the

BCA Assay Kit (P0010S, Beyotime, Shanghai, China). Protein samples were denatured by heating at 100 °C for 10 min. In addition, 8–12% SDS-PAGE gels were used to separate proteins (30 μg per lane), and then the proteins were electrotransferred to the polyvinylidene fluoride (PVDF) membranes. After blocking with 5% skim milk at room temperature for 1.5 h, the membranes were incubated overnight at 4 °C with primary antibodies. The following day, after being washed three times with TBST, the membranes were subsequently incubated for 1 h at room temperature with HRP-conjugated secondary antibodies. An ECL chemiluminescence solution (17047, Zenbio, Chengdu, China) was used to visualize, and Fusion software was used to conduct the semi-quantification of bands. The primary and secondary antibodies are presented in Additional File 1: Supplementary Table S3.

CCK-8 assay

The proliferation of HPMECs was assessed by a CCK-8 Assay Kit (C0037, Beyotime, Shanghai, China), which measured the optical density (OD) values at different times. In brief, 4×10^3 cells were counted and then seeded into 96-well culture plates with 100 μL of media per well. After incubating the cells, 10 μL of CCK-8 solution was added to each well, followed by incubation for 1–4 h. Absorbance at 450 nm was then detected using a microplate reader (FlexStation®3, Molecular Devices, California, USA).

EdU assay

Cell proliferation was analyzed using the EdU Cell Proliferation Kit with Alexa Fluor 488 (C0071S, Beyotime, Shanghai, China). After transfection and LPS stimulation, HPMECs were cultured with EdU working buffer for 2 h. Then, 4% paraformaldehyde (P0099, Beyotime, Shanghai, China) was used to fix the cells for 30 min at room temperature. After that, 0.3% Triton X-100 (P0096; Beyotime, Shanghai, China) was used to permeate the membranes of cells for 15 min. Afterward, HPMECs were cultured with 1×EdU click reaction mixture for 30 min in a dark environment. Hoechst33342 (C1027, Beyotime, Shanghai, China) was applied to stain the nuclei for another 10 min, and images were captured with a fluorescence microscope.

Scratch-wound healing assays

HPMECs, following transfection and LPS treatment, were subjected to a scratch-wound healing assay to assess cellular migration. A uniform scratch was made along the center of a 6-well plate using a 200 μL pipette tip. The cells were washed three times with prewarmed PBS, and then 2 mL of serum-free medium was added to each well to maintain the continued culture. The wound areas were recorded at 0 h and 24 h, and the migration was analyzed using ImageJ software.

Transwell migration assay

The migratory capacity of HPMECs was evaluated using a transwell migration assay. Approximately 1×10^4 cells were placed into the transwell insert upper chamber (8 μm pore size; Corning, NY, USA) with 200 μL of serum-free medium. The lower chamber was filled with 500 μL complete medium to serve as a chemoattractant. After 24 h of incubation, 4% paraformaldehyde was added to the transwell chambers to fix the

migrated cells for 15 min at room temperature. Cells were then stained with 0.4% crystal violet for 5 min. Images were captured by a microscope to quantify the migration.

Enzyme-linked immunosorbent assay (ELISA) assay

To evaluate the levels of inflammatory cytokines, cell culture medium supernatant and mice blood samples were collected and centrifuged at 1000×*g* for 10 min at 4 ℃. Following the protocols from the manufacturer, the concentrations of IL-1β (interleukin-1β) and IL-6 (interleukin-6) were quantified using enzyme-linked immunosorbent assay (ELISA) kits (ABclonal, Wuhan, China). Absorbance was promptly detected at 450 nm wavelength, and the concentrations of cytokines were calculated on the basis of standard curves according to the instructions of the product.

TUNEL assay

Apoptosis in both HPMECs and lung tissue sections (5 μm thickness) was measured using a one-step TUNEL Apoptosis Assay Kit (C1088, Beyotime, Shanghai, China) following the manufacturer's guidelines. Apoptotic cells were visualized under a fluorescence microscope after staining, and the images were processed and analyzed by ImageJ software.

RNA-seq

For transcriptomic analysis, HPMECs were first transfected with *TET2* siRNA or control siRNA, followed by LPS stimulation for 24 h. Total RNAs were harvested using TRIzol reagent to construct an RNA library. RNA sequencing was carried out on the Illumina Novaseq X Plus platform (Illumina, California, USA). Differentially expressed genes (DEGs) were identified on the basis of log2(fold-change) > 1 and an adjusted p-value ≤ 0.05.

Luciferase activity assay

The *ITGA10* full-length promoter fragment was cloned into the pGL4 basic promoter vector. A total 1×10^5 of HEK293T cells per well were plated in 48-well plates and cultured for 24 h. When the density of cells reached about 70% with better growth, the pGL4 basic promoter plasmid or the pGL4-*ITGA10* promoter plasmid (GenePharma, Shanghai, China) was applied to transfect cells by using GP-transfect-Mate (GenePharma, Shanghai, China). At the same time, the adenovirus empty constructs (EC) or the *TET2*-overexpressing adenovirus constructs with a multiplicity of infection of 80 were also used to transfect HEK293T cells. After 6 h, the transfection media were removed and replaced with fresh medium. After about 48 h of incubation, the firefly luciferase and the Renilla luciferase activities were measured by using the Dual-Luciferase® Reporter Assay System (E1910, Promega, Wisconsin, USA).

Methylation-specific PCR

DNA was extracted from cells by previous methods and then sodium bisulfite treatment was performed to convert unmethylated cytosine to uracil according to EZ DNA Methylation Kit instructions. Methylated DNA and unmethylated DNA were amplified with methylated primers and unmethylated primers, respectively. The PCR products were

loaded onto an agarose gel for electrophoresis. All primers were synthesized by Beijing Genomics Institute (Beijing, China), and these sequences are listed in Additional File 1: Supplementary Table S4.

Loci-specific 5-hmC qPCR

DNA was extracted from cells by previous methods. The 5-hmC level was detected with the BisulPlus™ Loci 5mC and 5hmC Detection PCR Kit (P1067, EpiGentek, New York, USA) by q-PCR. The primers were the same with specific methylation PCR (MSP). The relative 5-hmC abundance was calculated according to a previous study [35].

Hematoxylin and eosin (H&E)

The harvested fresh lung tissues were fixed in 4% paraformaldehyde, then embedded in paraffin, and sectioned at a thickness of 5 μm. Sections were stained with hematoxylin and eosin (H&E) and then imaged using a microscope (Olympus, Japan). Lung injury severity was evaluated using previously established criteria [36].

Immunofluorescence

The tissues were fixed in 4% paraformaldehyde, permeabilized with Triton X-100, and finally blocked with 5% BSA. Next, the samples were incubated with specific primary antibodies to the target protein at 4 °C overnight. Following washing with PBST, the samples were incubated with fluorescentdye-conjugated secondary antibodies. DAPI staining solution (C1005, Beyotime, Shanghai, China) was applied for nuclear staining. Fluorescence microscope was employed to capture and analyze the immunofluorescence images.

Bronchoalveolar lavage fluid (BALF) analysis

Subsequently, 24 h after CLP, the mice were sacrificed, and the lung tissues and BALF samples were collected for subsequent study. After centrifugation, the supernatant of BALF was collected and used for protein content analysis via the BCA method. In addition, the levels of cytokine (IL-1β and IL-6) were measured using ELISA Kits. Then, the total numbers of cells in BALF were counted using cell counting plates after BALF was suspended.

The wet/dry (W/D) weight ratio

To assess the water content of ALI lungs, one lobe of lungs from each mouse was taken to measure the wet weight (W), followed by desiccation in an oven at 65 °C for 24 h to measure the dry weight (D). The W/D weight ratio was calculated to evaluate lung tissue permeability and fluid accumulation.

Evans blue assay

The Evans blue dye assay was utilized to determine lung permeability in ALI mice, as reported previously [37]. Briefly, mice were anesthetized, and Evans blue dye (CM05086, Proteintech, Wuhan, China) was injected into the mice through the tail vein (45 mg/kg). About 2 h later, the dye reached the lung tissue through blood circulation. The harvest lung tissues were washed using saline to remove excess dye. Then, the lung tissues were

homogenized and the Evans blue (EB) dye extracted using a buffer solution. At last, the concentration of EB dye in the lung tissues was detected using a spectrophotometer.

Statistical analyses

Statistical analyses were performed using GraphPad Prism software (version 10.0.2, San Diego, CA, USA). Data were presented as mean ± standard deviation (SD). For two groups, the unpaired Student's *t*-test was utilized to analyze the data with equal variance, and Mann–Whitney test was used to analyze the data with unequal variance. For three or more groups, the one-way analysis of variance (ANOVA) and Tukey's multiple comparisons test were applied. The correlation between 5-hmC modification levels and apoptotic cell proportions in ALI tissues was analyzed using Spearman's correlation. A p-value < 0.05 was regarded as indicating statistical significance.

Results

Tet2 and 5-hmC levels were decreased and associated with increased apoptosis in sepsis-induced ALI mice model

To assess changes in 5-hmC modification levels during sepsis-induced ALI, we first established a sepsis-induced ALI mice model using the cecal ligation and puncture (CLP) surgery, which is the most accepted method for the establishment of sepsis models. Then, we verified the validity of our animal model with a series of experiments, including pathological injury, lung tissue permeability, inflammatory cytokines, and apoptosis levels (Additional File 1: Supplementary Fig. S2A–E). On the basis of these data above, our sepsis-induced ALI mice model was proved to be well established for the next analysis.

To further evaluate the 5-hmC modification levels in sepsis-induced ALI, a dot blot assay was conducted to measure the 5-hmC level changes in lung tissue harvested from both sham and CLP group. The results showed a noticeable decrease in 5-hmC levels in the CLP group (Fig. 1A). Interestingly, a negative correlation was observed between total 5-hmC levels and the apoptotic index in mouse lung tissue (Fig. 1B), suggesting that reduced 5-hmC modification might correlate with increased apoptosis in sepsis-induced ALI. Given that 5-hmC is primarily generated by the oxidation of 5-mC by TET family, we used RT-qPCR to evaluate the expression of *Tet1*, *Tet2*, and *Tet3* in the sham and CLP groups. We found a marked reduction in *Tet* expression, particularly *Tet2*, in the CLP group (Fig. 1C). Consistently, immunoblot results confirmed that Tet2 protein levels were also lower in the CLP group compared with the sham group (Fig. 1D). The results suggested that the downregulation of 5-hmC modification is dominantly regulated by *Tet2* in sepsis-induced ALI, instead of *Tet1* or *Tet3*. In addition, the expression and location of *Tet2* in mouse lung tissues were detected by immunofluorescence staining. As shown in Fig. 1E, we found that the expression of *Tet2* was decreased in the CLP group, and the cells with strong *Tet2* expression almost coincided with the positive cells of *Cd31*, which was specifically expressed by endothelial cells. The results suggested that *Tet2* was mainly expressed in pulmonary vascular endothelial cells, which implicates *Tet2*'s involvement in endothelial cell function during sepsis-induced ALI progression.

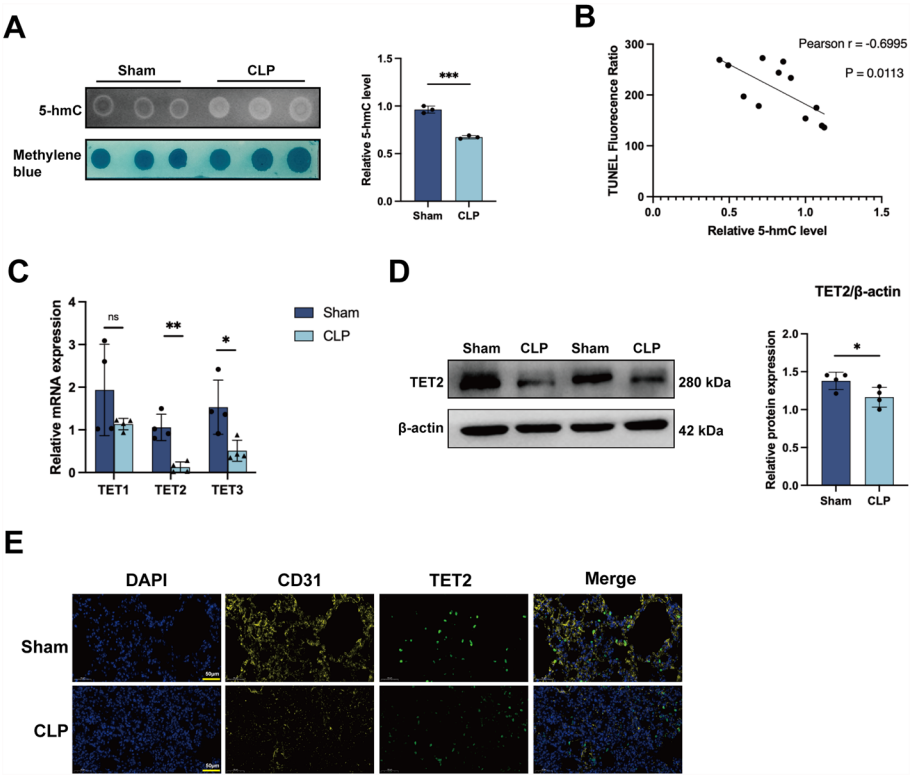

Fig. 1 The 5-hmC modification level and the expression of Tet2 in lung tissues after CLP surgery. **A** Total DNA 5-hmC modification levels in lung tissues were tested using 5-hmC DNA dot blot assay. **B** The relationship of DNA 5-hmC level with apoptosis in lung tissues was analyzed using Spearman correlation (Spearman $r = -0.6995$, $P = 0.0113$, $n = 12$). **C** *Tet1*, *Tet2*, and *Tet3* relative mRNA expression in lung tissues was detected by RT-qPCR, and *Gapdh* was served as loading control. **D** Relative protein expression of Tet2 in lung tissues was examined by immunoblot. **E** Immunofluorescence images of *Tet2* and *Cd31* in lung tissues from sham and CLP mice (scale bar: 50 μm). Data were expressed as mean ± standard deviation (mean ± SD). An unpaired Student's *t*-test was used for the comparison of data between the two groups. Spearman's correlation was performed to analyze the correlation between 5-hmC modification levels and apoptotic cell proportions in ALI tissues. $n = 3$–4 each group; *ns* no significance; $^{*}P < 0.05$; $^{**}P < 0.01$; $^{***}P < 0.001$

TET2 and 5-hmC levels were decreased in LPS-stimulated HPMECs, and TET2 deficiency aggravated HPMEC apoptosis

Besides the sepsis-induced ALI mice model, we also generated in vitro model to explore the effect of *TET2* under inflammatory conditions using HPMECs. we stimulated HPMECs with LPS for 0, 6, 12, and 24 h to assess the level of 5-hmC using a DNA dot blot. Consistent with previous in vivo study, 5-hmC expression was decreased at all time points post LPS stimulation (Fig. 2A). Next, we evaluated the mRNA levels of *TET* family members (*TET1*, *TET2*, *TET3*) in LPS-treated HPMECs. Still, *TET2* showed the most pronounced decline compared with *TET1* and *TET3* (Fig. 2B). Further, both mRNA expression and protein levels of TET2 were measured after 0, 6, 12, and 24 h of LPS treatment. The results indicated TET2 was decreased at all time points, especially at 12 h (Fig. 2C, D). To figure out the role of *TET2* in HPMECs, we used small interfering RNAs (siRNA) and an adenovirus vector to knock down and overexpress *TET2* in HPMECs. After validating the efficacy of knockdown and overexpression of *TET2* in HPMECs, TUNEL assay was performed. We discovered that the apoptosis in HPMECs treated with LPS increased upon *TET2* knockdown

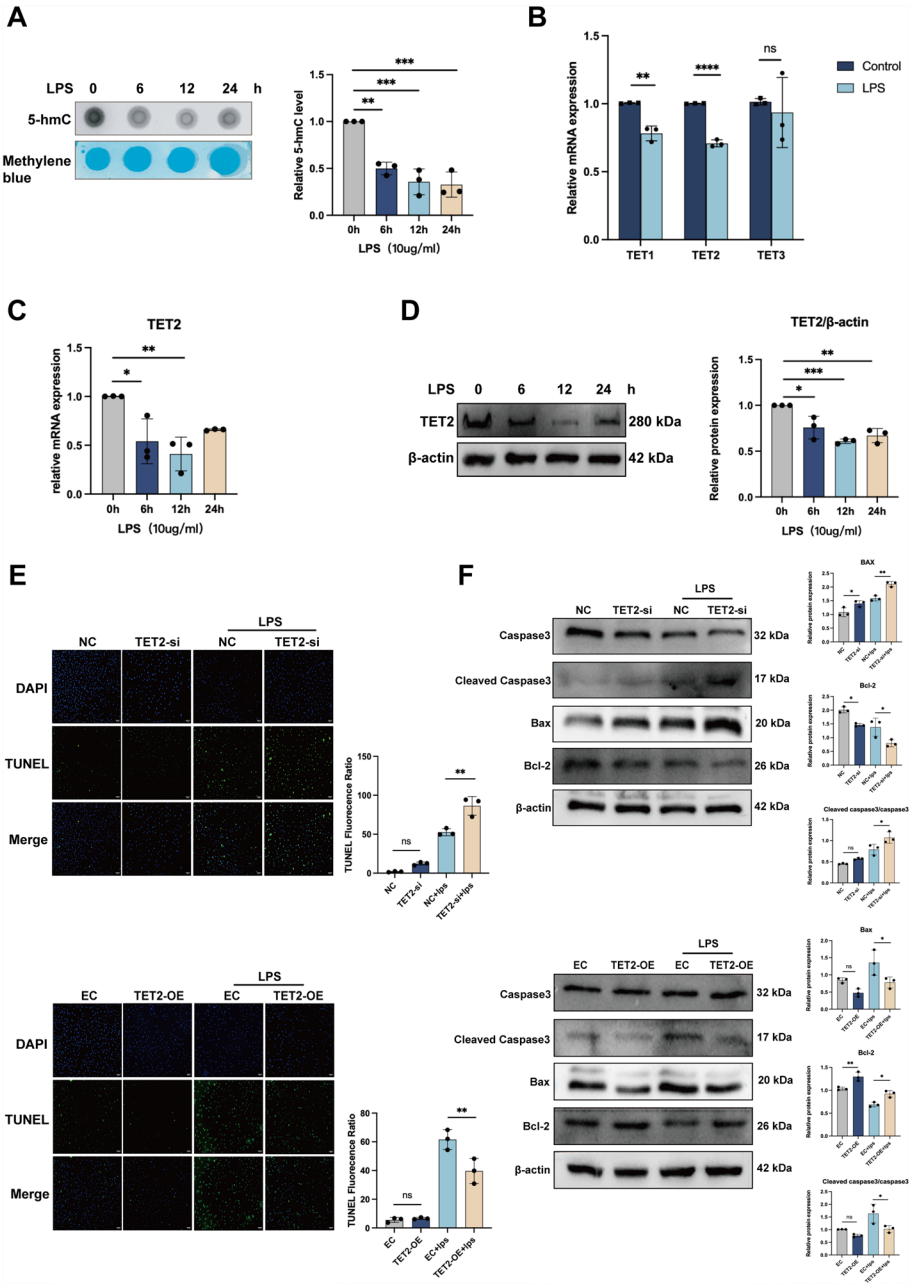

Fig. 2 LPS downregulated *TET2* expression in HPMECs, and *TET2* deficiency aggravated apoptosis of HPMECs under LPS-stimulation. **A** Differential 5-hmC level in HPMECs treated with LPS at different time points. **B** Relative mRNA expression of *TET1*, *TET2*, and *TET3* in HPMECs treated with LPS was detected by RT-qPCR, with *GAPDH* served as loading control. **C** Differential mRNA expression of *TET2* in HPMECs treated with LPS at different time points was detected by RT-qPCR. **D** Differential protein expression of TET2 in HPMECs treated with LPS at different time points. **E** Apoptosis of HPMECs treated with LPS was analyzed using TUNEL. **F** Immunoblot analysis of total Caspase3, Cleaved Caspase3, BAX, and BCL-2. β-actin was utilized as an internal control. Data were expressed as mean ± standard deviation (mean ± SD). An unpaired Student's *t*-test was performed to compare data between two groups. One-way ANOVA with Tukey's multiple comparisons test was used to compare multi-group data; $n = 3$ each group; *ns* no significance; *$P < 0.05$; **$P < 0.01$; ***$P < 0.001$; ****$P < 0.0001$

but was reduced when *TET2* was overexpressed (Fig. 2E). This was further supported by immunoblot analysis of critical apoptosis-related proteins. The results showed that *TET2* knockdown led to upregulation of Cleaved Caspase3 and BAX, while downregulating BCL-2. Conversely, *TET2* overexpression had the opposite effect, decreasing Cleaved Caspase3 and BAX and increasing BCL-2 expression (Fig. 2F). This multimodality analysis supports the conclusion that *TET2* plays a protective role in preventing apoptosis in HPMECs under inflammatory conditions through the inhibition of apoptosis signaling pathways.

TET2 regulates the dysfunction and inflammation of HPMECs treated with LPS

To figure out the potential effect of *TET2* on HPMECs function, we performed a series of experiments assessing cell proliferation, migration, and inflammation under conditions of *TET2* knockdown and overexpression. First, a CCK-8 assay was utilized to assess the proliferation of HPMECs. The results demonstrated that *TET2* knockdown impaired HPMEC proliferation, while it was enhanced when *TET2* was overexpressed, regardless of the presence of LPS stimulation (Fig. 3A). These findings were further confirmed using the EdU assay, where similar patterns were observed (Fig. 3B). Next, we measured the migration of HPMECs by scratch-wound healing assay. The cell migration area was markedly reduced in the LPS-stimulated group compared with the unstimulated group. Notably, *TET2* knockdown resulted in a marked reduction in cell migration, while overexpression of *TET2* enhanced the migratory capacity of HPMECs (Fig. 3C). These findings were further supported by the Transwell migration assay, which revealed a lower number of migrated cells following *TET2* knockdown, whereas *TET2* overexpression significantly promoted cell migration (Fig. 3D). We also examined whether *TET2* was involved in regulating endothelial barrier function by assessing the expression level of *VE-cadherin*, a critical intercellular junction protein. Immunoblot analysis showed that TET2 knockdown led to reduced VE-cadherin expression, while TET2 overexpression increased its expression (Fig. 3E). This suggests that *TET2* may participate in maintaining endothelial integrity. To explore the impact of *TET2* on inflammation in endothelial cells, we used RT-qPCR to measure the level of proinflammatory cytokines *IL-1β* and *IL-6*. The results indicated that the level of *IL-1β* and *IL-6* were significantly higher in *TET2* knockdown group, while these levels were lower in the *TET2* overexpression group. (Fig. 3F). Meanwhile, we also found similar results in human umbilical vein endothelial cells (HUVECs). The expression of TET2 decreased in LPS-stimulated HUVECs. After knockdown of TET2, the proliferation and migration abilities of HUVECs were weakened. However, after overexpression of TET2, the proliferation and migration abilities of HUVECs increased (Additional File 1: Supplementary Fig. S4A–C). Collectively, these data suggest that *TET2* is a critical regulator of endothelial dysfunction and inflammation in LPS-treated HPMECs. *TET2* appears to promote cell proliferation and migration, maintain endothelial barrier function, and modulate cellular inflammatory responses, positioning it as a key player in the endothelial response to sepsis.

Knockdown of Tet2 aggravates acute lung injury in septic mice by increasing inflammation and apoptosis

To examine the involvement of *Tet2* in sepsis-induced ALI, we utilized an AAV6 viral vector carrying *Tet2*-specific shRNA, which was administered to mice via tail vein injection. Subsequently, 4 weeks after injection, the efficiency of *Tet2* knockdown

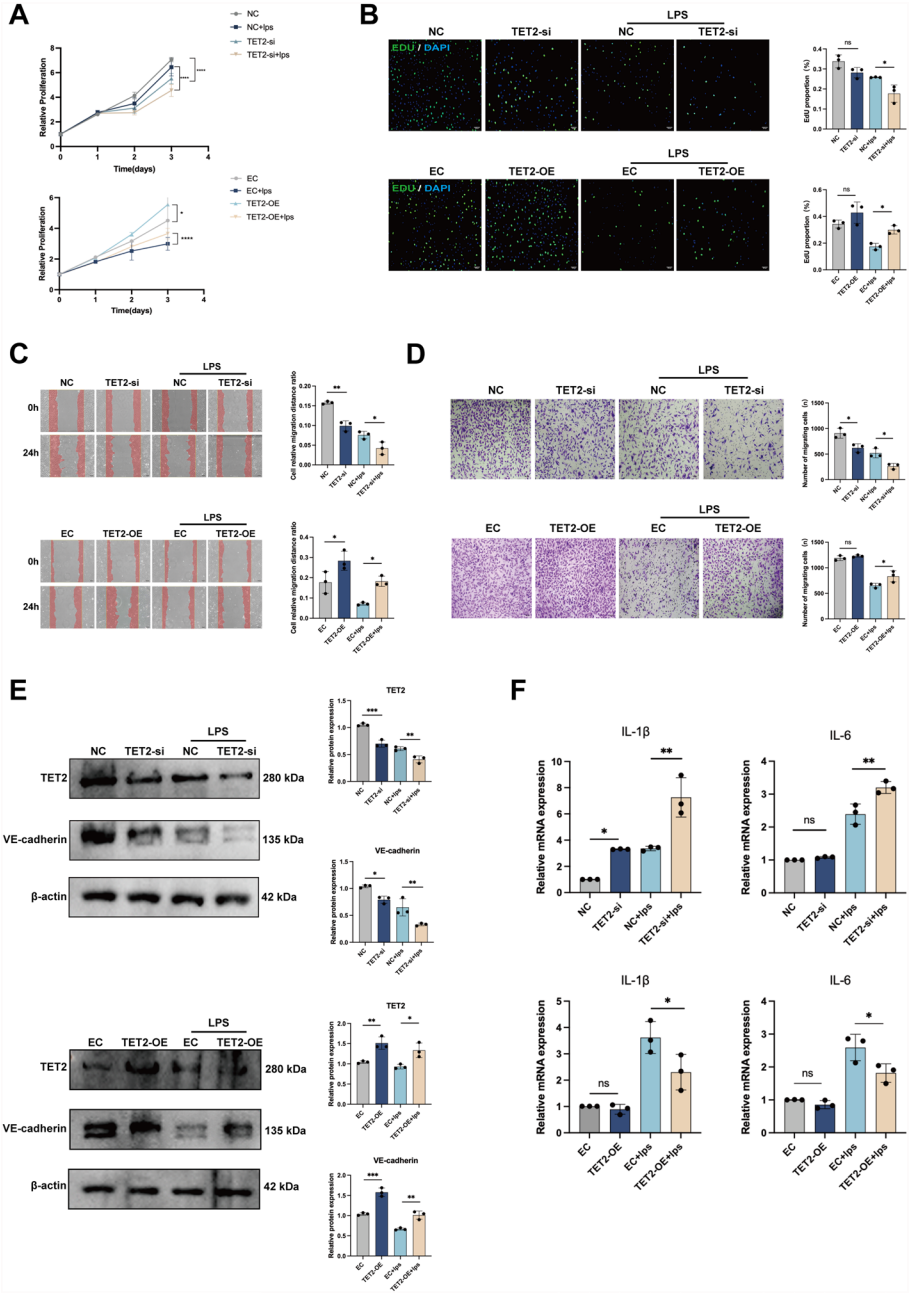

Fig. 3 *TET2* regulates the LPS-stimulated dysfunction of HPMECs. **A, B** The proliferation of HPMECs under silencing or overexpressing *TET2* was detected using CCK-8 and EdU assay. **C, D** The migration ability of HPMECs under silencing or overexpressing *TET2* was measured using scratch-wound healing assay and Transwell migration assay. **E** The protein expression level of VE-cadherin and TET2 under silencing or overexpressing *TET2*. **F** The levels of *IL-1β* and *IL-6* under silencing or overexpressing *TET2* were detected using RT-qPCR. Data were expressed as mean ± standard deviation (mean ± SD). An unpaired Student's *t*-test was performed to compare data between two groups. One-way ANOVA with Tukey's multiple comparisons test was used to compare multi-group data; $n = 3$ each group; *ns* no significance; $^{*}P < 0.05$; $^{**}P < 0.01$; $^{***}P < 0.001$; $^{****}P < 0.0001$

was validated by immunoblot analysis (Fig. 4A, B). Meanwhile, we verified the knockdown efficiency of *Tet2* in mouse lung tissues using immunofluorescence staining (Additional File 1: Supplementary Fig. S1F). Subsequently, a DNA dot blot was performed to measure the level of 5-hmC in the lung tissues of mice. As expected, the levels of 5-hmC were reduced in CLP mice and were further decreased in *Tet2* knockdown CLP mice, with no notable difference between the CLP and NC + CLP groups (Fig. 4C). Histopathological analysis using H&E staining revealed that knocking down *Tet2* exacerbated pathological changes in lung tissues. *Tet2* knockdown CLP mice displayed more severe destruction of alveolar and bronchial structures, increased leukocyte infiltration, and thickening of the alveolar septa compared with CLP mice (Fig. 4D). Moreover, we used Evans blue staining and W/D weight ratio to measure the permeation of lung tissue. Both methods demonstrated that the lung tissue permeability was further decreased in *Tet2* knockdown CLP mice compared with CLP mice. In addition, analysis of BALF further revealed that both total cell numbers and total protein levels were significantly elevated following *Tet2* knockdown (Fig. 4E). Given the critical role of *VE-cadherin* in maintaining endothelial barrier integrity, we evaluated its expression in vivo using immunoblot analysis. We found that VE-cadherin expression was further reduced in *Tet2*-deficient mice compared with CLP mice (Fig. 4F). To assess the impact of *Tet2* knockdown on endothelial inflammation, we measured the levels of proinflammatory cytokines IL-1β and IL-6 using ELISA and qPCR. Compared with the CLP mice, these cytokines were significantly upregulated in *Tet2* knockdown CLP mice (Fig. 4G). Moreover, apoptotic proteins were also examined, revealing that *Tet2* knockdown led to an increase in apoptosis in sepsis-induced ALI. Immunoblot analysis suggested that *Tet2* knockdown upregulated apoptotic protein expression, including cleaved caspase-3 and Bax and downregulated Bcl-2 expression, which is an anti-apoptotic protein (Fig. 4H). Consistent with these findings, TUNEL staining also showed an increase in apoptotic cells in the *Tet2* knockdown CLP mice group compared with the CLP mice group (Fig. 4I). Overall, these results indicated that suppressing the expression of *Tet2* can significantly exacerbate sepsis-induced lung injury by promoting inflammation and apoptosis.

(See figure on next page.)

Fig. 4 Knockdown of *Tet2* aggravates acute lung injury in septic mice. **A** The diagram of the mice experimental procedure. AAV6-shRNA viral vector targeting *Tet2* and negative control gene (NC) were constructed and injected 4 weeks before CLP surgery via the tail vein of the mice. Bood, BALF, and lung tissues of mice were collected 24 h after CLP surgery for subsequent detection. **B** The efficiency of *Tet2* knockdown in lung tissue was confirmed by immunoblot. **C** The total DNA 5-hmC modification level in lung tissue after CLP was detected by the 5-hmC dot blot assay. **D** Representative H&E staining images of CLP lung tissue sections and the lung injury score (scale bar: 50 μm). **E** EB staining and W/D weight ratio was used to measure the permeability of lung tissues of mice. The number of cells in mouse BALF were counted. The total protein levels in BALF of mice were detected by BCA method. **F** Immunoblot was used to measure the protein expression of Ve-cadherin. β-actin served as internal control. **G** RT-qPCR and ELISA were used to measure the level of *IL-1β* and *IL-6* in lung tissues and plasma. *Gapdh* was applied as loading control. **H** Immunoblot was used to measure the protein expression changes of caspase3, cleaved caspase3, Bax, and Bcl-2. **I** TUNEL staining was used to detect apoptosis in lung tissues (scale bar: 100 μm). Data were expressed as mean ± standard deviation (mean ± SD). An unpaired Student's *t*-test was performed to compare data between the two groups. One-way ANOVA with Tukey's multiple comparisons test was used to compare multi-group data; $n = 3–4$ each group; *ns* no significance; *$P < 0.05$; **$P < 0.01$; ***$P < 0.001$; ****$P < 0.0001$

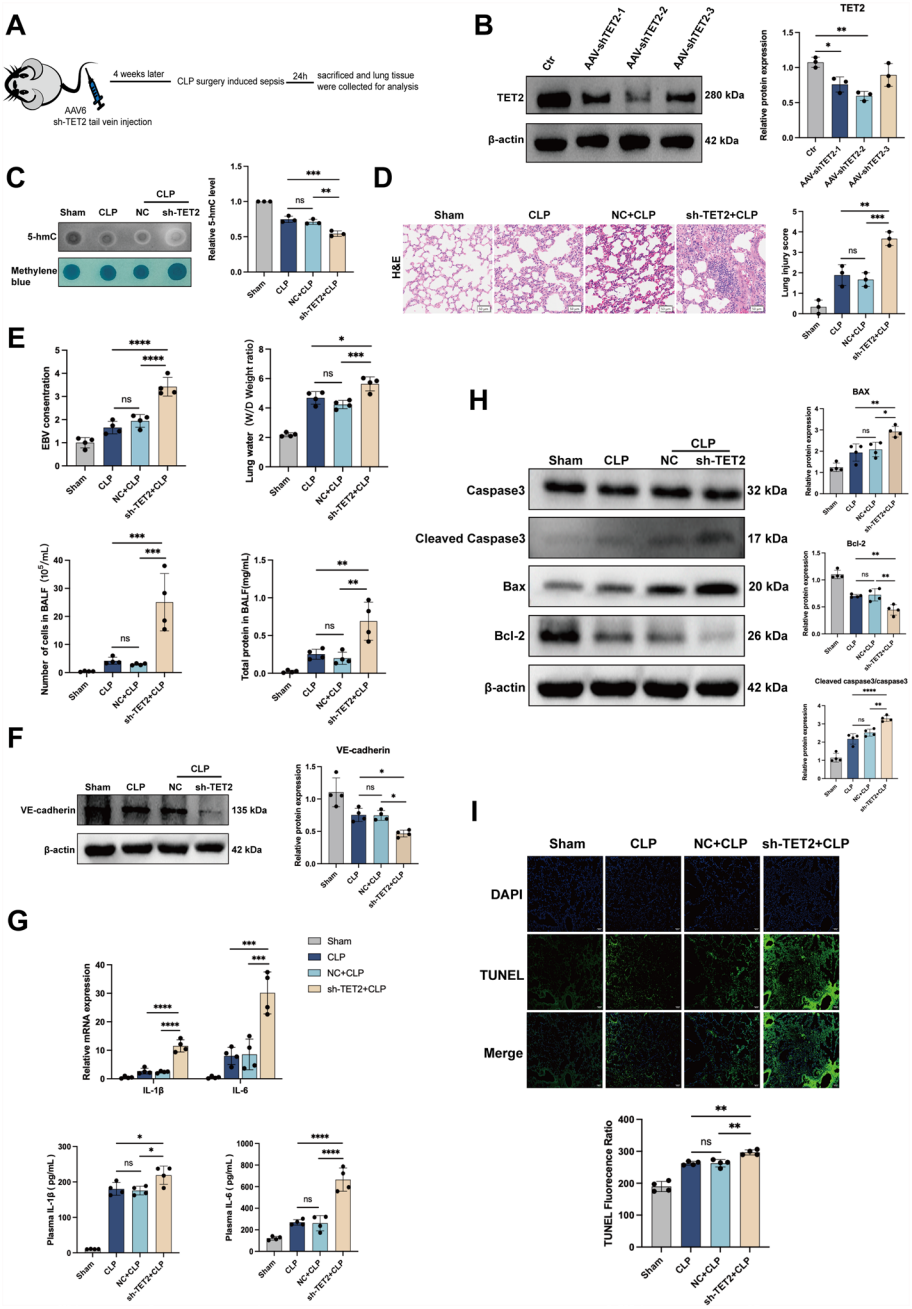

Fig. 4 (See legend on previous page.)

TET2 regulated PI3K-AKT signaling pathway by targeting ITGA10

The data detailed above validated that *TET2* function is important for the sepsis-induced ALI. Hence, in the investigation for the mechanism underlying this impact on HPMECs under LPS stimulation, we further studied the potential target genes regulated by *TET2*. Initially, RNA-seq was performed on HPMECs treated with *TET2* siRNA group and NC siRNA to explore the potential target genes (Fig. 5A). The analysis showed that there were 110 upregulated and 123 downregulated genes upon *TET2* suppression (Fig. 5B). Then we applied Kyoto Encyclopedia of Genes and Genomes (KEGG)

enrichment analysis to confirm the signaling pathways enriched by genes related to *TET2*. Pathway analysis showed that *TET2* knockdown had critical effects on genes that are related to extracellular matrix (ECM)-receptor interaction, focal adhesion, and the PI3K-AKT pathway, which are crucial for cell proliferation, migration, and adhesion [38, 39] (Fig. 5C). KEGG analysis suggested that the PI3K-AKT pathway is the intersection of the above three pathways, prompting us to focus on the differential genes within the PI3K-AKT pathway. It is well known that *TET2* levels positively regulate the expression of its downstream genes. Our KEGG analysis identified three integrin genes (*ITGA7*, *ITGA10*, and *ITGA11*) as being positively correlated with *TET2*, leading us to prioritize these candidates for further validation. In our in vivo and in vitro models, we discovered a decrease in *TET2* levels, followed by an examination of *ITGA7*, *ITGA10*, and *ITGA11*, all of which were downregulated following *TET2* knockdown. To validate the findings, we detected the change of these genes in mRNA level by RT-qPCR under silencing or overexpressing *TET2* in HPMECs. In preliminary validation experiment, we found that these three genes' expression levels were positively related to *TET2*, and the expression of *ITGA10* was most closely associated with the expression of *TET2* among these genes (Fig. 5D). We did further immunoblot experiment to confirm the expression changes of ITGA10 at protein level and observed that the expression of ITGA10 was positively correlated with TET2 expression. These results suggested that *ITGA10* might be a target gene regulated by *TET2* (Fig. 5E). To obtain direct evidence of *TET2* regulating *ITGA10*, we performed a luciferase reporter assay, which demonstrated that the activity of *ITGA10* promoter was enhanced by *TET2* (Fig. 5F). To further verify whether TET2 can regulate ITGA10 methylation levels, we used specific methylation PCR (MSP) to detect ITGA10 methylation. The results of the MSP experiment suggested that the methylation level of ITGA10 promoter decreased after TET2 overexpression compared with the control group (Fig. 5G). To verify whether the methylation change of ITGA10 promoter regulated by TET2 is mediated by 5-hmC modifications, we used loci-specific 5-hmC qPCR kit to detect the 5-hmC abundance of ITGA10 promoter, and the results suggested that the 5-hmC abundance of ITGA10 promoter increased after overexpression of TET2 (Fig. 5H). It is commonly known that the PI3K-AKT signaling pathway is involved in endothelial dysfunction during inflammatory responses. Recent studies have shown that *ITGA10* activates the PI3K-AKT pathway in some diseases [40, 41]. Thus, we hypothesized that *TET2* modulates the PI3K-AKT signaling pathway through *ITGA10* in our HPMECs model. Therefore, we detected the changes of phosphorylation levels of PI3K and AKT in both in vivo and in vitro. The immunoblot results showed that *TET2* knockdown led to the reduction of the phosphorylation level of PI3K and AKT, while *TET2* overexpression had the opposite effects (Fig. 5I). In conclusion, our findings support the notion that *TET2* regulates the PI3K/AKT signaling pathway by positively modulating *ITGA10* expression, thereby influencing endothelial cell functions and inflammatory responses.

Knockdown of ITGA10 weakens the beneficial effect of TET2 overexpression on alleviating dysfunction and inflammation of HPMECs treated with LPS

Our previous results demonstrated that *TET2* is essential for alleviating dysfunction and inflammation of LPS-treated HPMECs, partly by activating the expression of *ITGA10*.

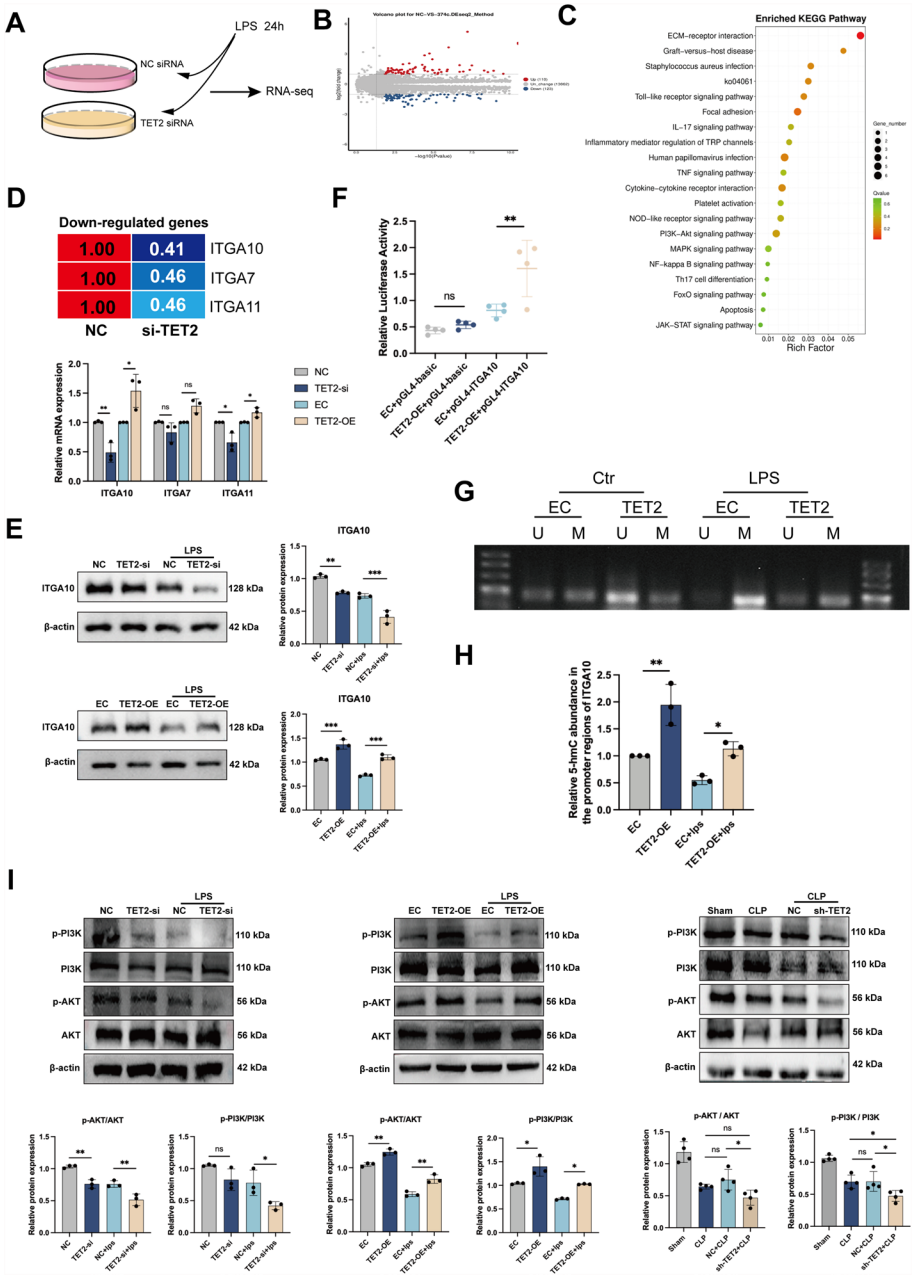

Fig. 5 *TET2* regulates PI3K-AKT signaling pathway by targeting *ITGA10*. **A** The diagram of sample preparation for RNA-seq. **B** Volcano plots are used to illustrate DGEs for HPMECs transfected with *TET2* siRNA or NC siRNA. **C** KEGG enrichment analysis identifies the signaling pathways associated with *TET2* regulated-genes. **D** Downregulated genes related to the integrin family were identified and their mRNA expression was validated by RT-qPCR. **E** Immunoblot was used to measure the protein level of ITGA10 with *TET2* knockdown or overexpression. β-actin served as internal control. **F** Luciferase reporter assay was used to examine the relative luciferase activities in HEK 293 T cells. **G** MSP was used to detect the methylation level of ITGA10 promoter after TET2 overexpression. **H** Loci-specific 5-hmC qPCR was used to detect the abundance of 5-hmC in ITGA10 promoter after TET2 overexpression. **I** The protein levels of total and phosphorylated AKT and PI3K were analyzed by immunoblot with *TET2* knockdown or overexpressed in vivo and in vitro. Data were expressed as mean ± standard deviation (mean ± SD). An unpaired Student's *t*-test was performed to compare data between two groups. One-way ANOVA with Tukey's multiple comparisons test was used to compare multi-group data; $n = 3–4$ each group; *ns* no significance; $^{*}P < 0.05$; $^{**}P < 0.01$; $^{***}P < 0.001$

We first explored the role of ITGA10 in HPMEC dysfunction, and we found that ITGA10 may play a protective role (Additional File 1: Supplementary Fig. S3A–D). Then we subjected HPMECs to *ITGA10* siRNA to generate *ITGA10* transient suppression condition for the ensuing studies. After the efficiency of *ITGA10* siRNA was confirmed by immunoblot analysis (Additional File 1: Supplementary Fig. S1E), we firstly used adenovirus to overexpress *TET2* in HPMECs and then suppressed *ITGA10* expression using siRNA in *TET2*-overexpressed HPMECs to investigate whether *ITGA10* deficiency could weaken the activation of PI3K-AKT pathway induced by *TET2* overexpression. We found that in the group with knockdown ITGA10 after TET2 overexpression (*TET2*-OE + *ITGA10*-si group), the activation of the PI3K-AKT pathway was decreased compared with the *TET2*-OE group (Fig. 6A). To evaluate inflammation, we measured the levels of proinflammatory cytokines *IL-1β* and *IL-6* using RT-qPCR. We found that the cytokine levels were higher in the *TET2*-OE + *ITGA10*-siRNA group compared with the *TET2*-OE group, indicating that ITGA10 knockdown reduced the antiinflammatory effect of *TET2* overexpression (Fig. 6B). Functional assays, including CCK-8 and EdU, demonstrated that the proliferation of HPMECs was significantly reduced in the *TET2*-OE + *ITGA10*-siRNA group compared with the *TET2*-OE group (Fig. 6C, D). Furthermore, cell migration assay, such as the scratch-wound healing assay and Transwell migration assays, revealed that the cell migration ability was markedly decreased in the *TET2*-OE + *ITGA10*-si group compared with the *TET2*-OE group (Fig. 6E, F). Lastly, we evaluated the expression of VE-cadherin, an essential protein involved in maintaining endothelial barrier integrity. The immunoblot results indicated that VE-cadherin expression was significantly reduced in the *TET2*-OE + *ITGA10*-siRNA group compared with the *TET2*-OE group (Fig. 6G). On the basis of the results above, we speculated that *TET2* alleviates the dysfunction and inflammation of HPMECs by targeting *ITGA10* via the PI3K-AKT signaling pathway, and knockdown of *ITGA10* diminishes the beneficial effects of *TET2* overexpression in LPS-stimulated endothelial cells (Fig. 7).

Discussion

Several studies have shown that epigenetic modifications are involved in sepsis [8]. However, the specific role of TET proteins, particularly TET2, in sepsis-induced ALI has not been thoroughly explored. In this study, we discovered that the level of *TET*s and 5-hmC modification were decreased in both in vivo and in vitro models of sepsis-induced ALI. Among three TET proteins, TET2 was validated as the dominant regulator for 5-hmC modification in sepsis-induced ALI. We further demonstrated that *TET2* could upregulate the expression of *ITGA10* via promoter activating and then active PI3K-AKT pathway in HPMECs. As far as we know, this is the first study to elucidate TET2's role in endothelial dysfunction in sepsis-induced ALI via epigenetic regulation of ITGA10.

The TET protein family, including TET1, TET2, and TET3, function as key epigenetic regulators by catalyzing the conversion of 5-mC to 5-hmC, thereby influencing various biological processes [21, 42]. In our study, we observed that *TET2* predominantly regulated 5-hmC levels in sepsis-induced ALI, while *TET1* and *TET3* contributed less significantly. Compared with *TET1* and *TET3*, *TET2* is the most closely related to inflammation and immunity [21]. Previous research has demonstrated the multifaceted role of *TET2* in regulating hematopoiesis [19], inflammation [21–26]

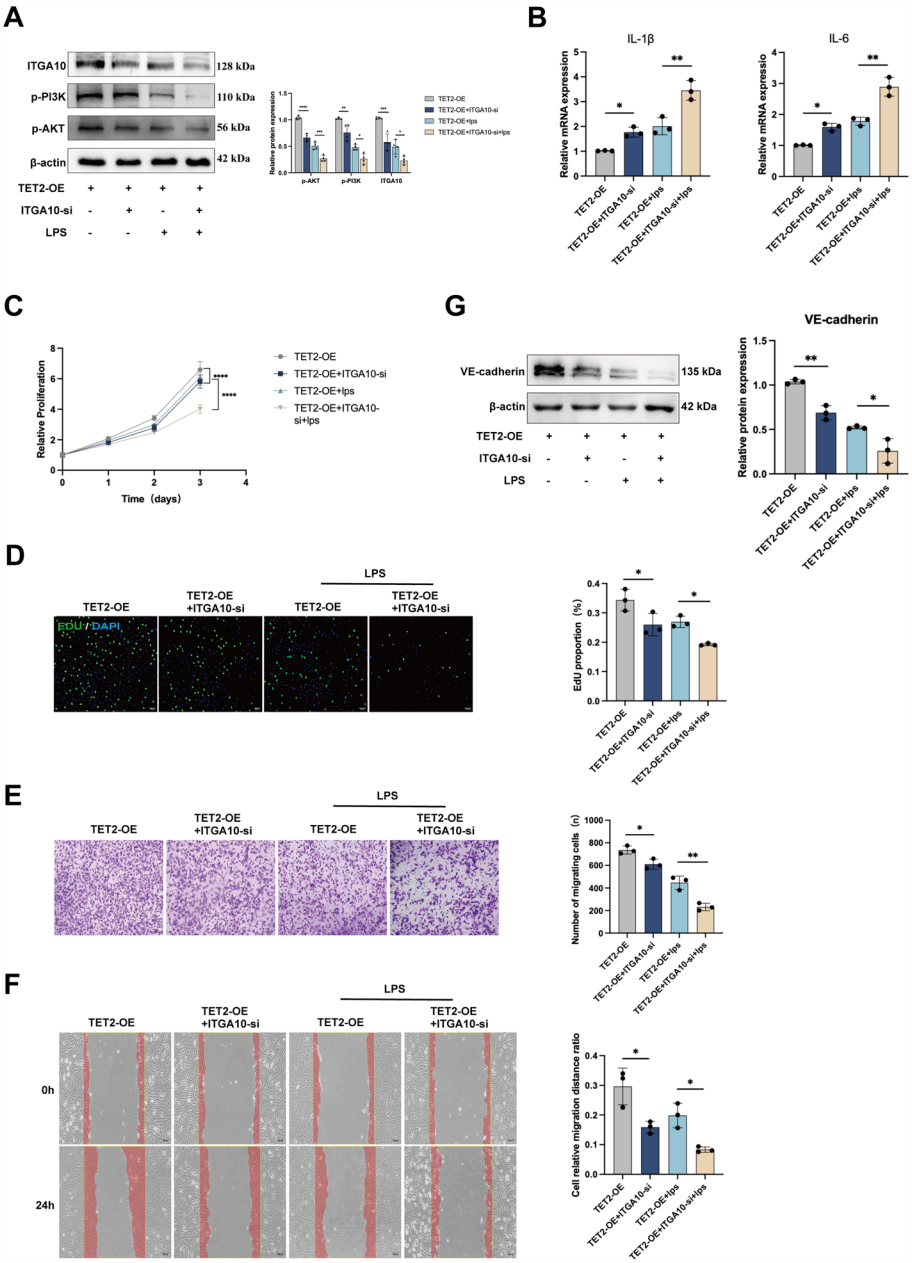

Fig. 6 Suppression of *ITGA10* weakens the beneficial effect of *TET2* overexpression on alleviating dysfunction of HPMECs treated with LPS. **A** Immunoblot was used to measure the protein expression levels of p-AKT and p-PI3K under silencing *ITGA10*. β-actin served as internal control. **B** RT-qPCR was used to detect the level of *IL-1β* and *IL-6*. **C, D** CCK-8 and EdU assay were used to detect the proliferation of HPMECs. **E, F** The migration ability of HPMECs under silencing *ITGA10* was examined using scratch assay and Transwell migration assay. **G** The protein expression level of VE-cadherin under silencing *ITGA10* was measured by immunoblot. TET2-OE + ITGA10-si group means the group with knockdown ITGA10 after TET2 overexpression. Data were expressed as mean ± standard deviation (mean ± SD). An unpaired Student's *t*-test was performed to compare data between two groups. One-way ANOVA with Tukey's multiple comparisons test was used to compare multi-group data; $n = 3$–4 each group; *ns* no significance; $^{*}P < 0.05$; $^{**}P < 0.01$; $^{***}P < 0.001$; $^{****}P < 0.0001$

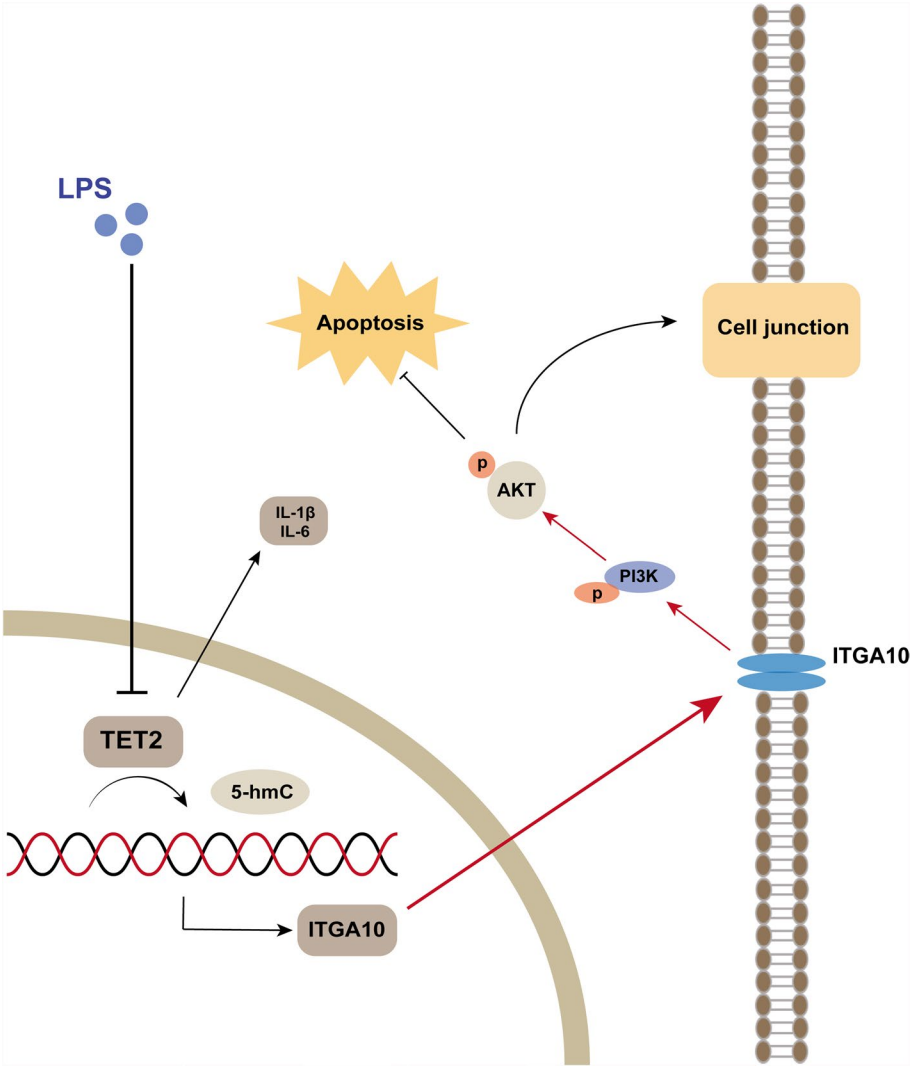

Fig. 7 Illustration of mechanism. *TET2* deficiency can aggravate the apoptosis and inflammation of LPS-treated HPMECs. Loss of *TET2* reduces the expression of *ITGA10*, thereby weakening the activity of the PI3K-AKT signaling pathway, promoting dysfunction of pulmonary vascular endothelial cells and exacerbating the symptoms of sepsis-induced acute lung injury

and pulmonary diseases [27–29]. Since a study published in *Nature* revealed that *Tet2* can repress *Il-6* to resolve inflammation, and *Tet2*-deficient mice exhibit strong IL-6 secretion capacity, a more severe inflammatory phenotype, and an increased risk of endotoxin shock [26], *Tet2* has begun to gain attention for its regulation in inflammation diseases. In addition, a study has demonstrated that acute kidney injury (AKI) induced by cisplatin is associated with *Tet2*. Bao et al. found that *Tet2*-knockout (KO) mice developed more severe kidney injury, and that *Tet2* protects the kidneys from damage by regulating inflammatory responses and metabolism through PPAR signaling pathway [20].

Previous studies have confirmed that sepsis-induced by CLP is a classic and widely used animal model for the study of sepsis-induced ALI. The progression and

characteristics of multi-bacterial sepsis induced by CLP are very similar to those of human sepsis [43]. Compared with other induction models, the CLP model can better reflect the complexity of human sepsis. Herein, on the basis of CLP-induced septic mice model, we firstly discovered that the level of 5-hmC and the expression of *Tet* family were declined in sepsis-induced ALI mice, especially *Tet2* given that *Tet2* was downregulated in the lung tissue of ALI mice, and the 5-hmC modification was negatively correlated with apoptosis of mouse lung tissue in our study. Subsequently, we used AAV6 to knock down *Tet2* in mice and discovered that *Tet2* deficiency aggravated the sepsis-induced ALI, marked by increased lung pathological injury and permeability of lungs, inflammation, and apoptosis. To better explore the effect of *Tet2* in sepsis-induced ALI, we detected the localization of *Tet2* in lung tissues. The result showed that *Tet2* was mainly expressed in pulmonary vascular endothelial cells, suggesting its significant involvement in maintaining endothelial cell integrity during sepsis-induced ALI.

HPMECs are one of the most important effector cells in sepsis-induced ALI. The dysfunction of endothelial cells is a hallmark of sepsis-induced ALI, leading to increased vascular permeability, pulmonary edema, and respiratory failure. Endothelial cell dysfunction is usually accompanied by abnormal endothelial cell activation and changes in cell migration and permeability [44]. In our in vitro experiments with LPS-treated HPMECs, *TET2* knockdown reduced cell proliferation, migration, and barrier function, while enhancing apoptosis and proinflammatory cytokine production (*IL-1β* and *IL-6*). Conversely, overexpression of *TET2* significantly alleviated these dysfunctions, indicating its protective role in maintaining endothelial cell function under septic conditions.

On the basis of our results, we sought to explore the mechanistic role of *TET2* in sepsis-induced ALI. It is well established that *TET2* regulates the expression of downstream target genes by modulating promoter methylation level to exert its function [45]. Subsequently, we performed RNA sequencing to identify the target genes and possible signaling pathways regulated by *TET2* in sepsis-induced ALI. The RNA-seq screened out 223 DGEs and these genes, related to *TET2*, were mainly enriched in pathways associated with cell adhesion and inflammatory response, including ECM-receptor interaction, focal adhesion, PI3K-AKT, IL-17, and NOD-like receptor signaling pathways, especially ECM-receptor interaction, focal adhesion, and PI3K-AKT, which were mainly concentrated in cell adhesion. ECM-receptor interaction refers to the interaction between extracellular matrix and receptors on the cell surface to trigger cell signal transduction pathways and affect biological functions such as cell migration, proliferation, differentiation, and apoptosis. Recent studies have confirmed that ECM-receptor interaction is involved in the occurrence and development of sepsis-induced ALI [46]. Focal adhesion is critical for maintaining endothelial barrier integrity and plays a key role in protecting lung function [47]. We used KEGG analysis to conduct a deeper excavation and found that the PI3K-AKT pathway is the intersection of the above pathways. Through further investigation, we found that ECM activates FAK in focal adhesion pathway by interacting with integrin receptors on the cell surface, which in turn activates the PI3K-AKT pathway [48–50], so we further focused on the effects of TET2 on the PI3K-AKT pathway. The activation of PI3K-AKT signaling pathway has been proved by many studies to be associated with sepsis-induced ALI and pulmonary endothelial dysfunction [51, 52],

which can regulate endothelial cell apoptosis, proliferation, inflammatory responses, and reverse cell dysfunction [53]. Using immunoblot analysis, we discovered that the activation of PI3K/AKT pathway was decreased by *TET2* knockdown and increased by *TET2* overexpression.

To find the target genes regulated by *TET2*, we paid close attention to the differential genes in the PI3K-AKT pathway. Then we discovered a total of five differential genes enriched in the PI3K-AKT pathway, including two upregulated genes and three downregulated genes. Generally, the level of *TET2* is positively correlated with gene expression. Combined with the results that the expression levels of *TET2* were both decreased in both in vivo and in vitro models, we noticed the three downregulated genes (*ITGA7*, *ITGA10*, *ITGA11*). After the preliminary validation experiment, we observed that only the mRNA expression level of these genes (*ITGA7*, *ITGA10*, *ITGA11*) was positively correlated with the level of *TET2*. We discovered that the expression changes of ITGA10 were most closely related to *TET2* by RT-qPCR, and immunoblot also verified this result. Meanwhile, we found the promoter activity of *ITGA10* was promoted, and the methylation level of *ITGA10* promoter was decreased by overexpressing *TET2*. We further found that the abundance of 5-hmC on ITGA10 promoter increased after overexpression of TET2. These results suggest that TET2 reduces the methylation level of ITGA10 promoter by increasing its 5-hmC level, thus promoting its expression.

ITGA10 (Integrin α10), a member of integrin α family, is known to promote cellular processes such as migration, proliferation, adhesion, and differentiation through the PI3K-AKT pathway [40, 41] and may contribute to endothelial function [54]. Goyer et al. discovered that *ITGA10* is involved in Fuchs endothelial corneal dystrophy development [55]. Our KEGG analysis also suggested that *ITGA10* is related to PI3K-AKT signaling pathway. Importantly, knocking down *ITGA10* in cells overexpressing *TET2* attenuated PI3K-AKT pathway activation. Therefore, we conclude that *TET2* deficiency aggravates endothelial cell dysfunction and promotes acute lung injury by targeting *ITGA10* via the PI3K-AKT pathway. In our study, we demonstrated that *ITGA10* is a downstream target gene of *TET2*, which may play a critical role in the endothelial cell dysfunction of sepsis-induced ALI.

Despite these insights, there are still some issues that need to be discussed further. Firstly, the 5-hmC modification level is mediated by TETs. In our in vivo and in vitro models, we found that the expression of TET2 decreased most significantly. Although TET2 is more closely related to inflammation and immunity than TET1 and TET3, the involvement of TET1 and TET3 in 5-hmC modification changes in sepsis-induced ALI cannot be ruled out, which requires further investigation. Secondly, the conditional knockout mice would probably provide more robust evidence for the role of *Tet2* in sepsis-induced ALI. While we focused on *ITGA10* and the PI3K-AKT pathway, there may be additional *TET2*-regulated genes and pathways involved in endothelial dysfunction during sepsis-induced ALI that we have not yet identified based on our present data.

Conclusions

Our research reveals a new perspective on the role of *TET2* in the progression of sepsis-induced ALI. We demonstrate that *TET2* deficiency aggravates lung injury by targeting *ITGA10* and suppressing the PI3K-AKT signaling pathway. These findings

indicate that *TET2* may be a promising therapeutic target for treating sepsis-induced ALI, highlighting its role in regulating endothelial cell function during inflammatory responses.

Abbreviations

ALI	Acute lung injury
TET2	Ten-eleven translocation protein 2
CLP	Cecal ligation and puncture
LPS	Lipopolysaccharide
HPMECs	Human pulmonary microvascular endothelial cells
HUVECs	Human umbilical vein endothelial cells
ITGA10	Integrin α10
ARDS	Acute respiratory distress syndrome
5-hmC	5-Hydroxymethylcytosine
5-mC	5-Methylcytosine
DNMT	DNA methyltransferase
AML	Acute myeloid leukemia
MDS	Myelodysplastic syndrome
DCs	Dendritic cells
PAH	Pulmonary arterial hypertension
COPD	Chronic obstructive pulmonary disease
Gpx4	Glutathione peroxidase 4
ELISA	Enzyme-linked immunosorbent assay
TUNEL	Terminal deoxynucleotidyl transferase dUTP nick end labeling
BALF	Bronchoalveolar lavage fluid
EB	Evans blue
OD	Optical density
IL-1β	Interleukin-1β
IL-6	Interleukin-6
KEGG	Kyoto Encyclopedia of Genes and Genomes
ECM	Extracellular matrix
DEGs	Differentially expressed genes

Supplementary Information

The online version contains supplementary material available at https://doi.org/10.1186/s11658-025-00739-1.

Supplementary Material 1.

Acknowledgements
We would like to extend our gratitude to the members of the Experimental Research Center at the First Affiliated Hospital of Chongqing Medical University for their support and express our sincere thanks to the team from Professor Tingxiu Xiang's lab in Chongqing University Cancer Hospital for their valuable advice and help on this project.

Author contributions
Hongxue Fu and Bin Gao analyzed the data, organized figures, and drafted the first manuscript; Hongxue Fu, Bin Gao, Xin Zhou, and Ailin Lan performed the experiments; Chang Liu contributed to literature research and background editing. Fachun Zhou and Jingyi Tang designed and supervised the study. All authors read and approved the final manuscript.

Funding
This work was supported by the Science and Technology Commission of Chongqing (cstc2021ycjh-bgZXM0129).

Availability of data and materials
The data supporting the conclusions of this study are available from the corresponding author on reasonable request.

Declarations

Ethics approval and consent to participate
All animal experiments were approved by the Ethics Committee on Animal Research of Chongqing Medical University (approval no. IACUC-CQMU-2024-0706, 20 September 2024) and performed in accordance with the Basel Declaration.

Consent for publication
Not applicable.

Competing interests
The authors state that they have no known competing personal relationships or financial interests that could have appeared to influence the work reported in this study.

Received: 1 November 2024 Accepted: 6 May 2025
Published online: 19 May 2025

References

1. Cecconi M, Evans L, Levy M, Rhodes A. Sepsis and septic shock. Lancet. 2018;392(10141):75–87.
2. Rudd KE, Johnson SC, Agesa KM, Shackelford KA, Tsoi D, Kievlan DR, et al. Global, regional, and national sepsis incidence and mortality, 1990–2017: analysis for the global burden of disease study. Lancet. 2020;395(10219):200–11.
3. Aziz M, Ode Y, Zhou M, Ochani M, Holodick NE, Rothstein TL, et al. B-1a cells protect mice from sepsis-induced acute lung injury. Mol Med. 2018;24(1):26.
4. Joffre J, Hellman J, Ince C, Ait-Oufella H. Endothelial responses in sepsis. Am J Respir Crit Care Med. 2020;202(3):361–70.
5. Vassiliou AG, Kotanidou A, Dimopoulou I, Orfanos SE. Endothelial damage in acute respiratory distress syndrome. Int J Mol Sci. 2020;21(22):8793.
6. Hattori Y, Hattori K, Machida T, Matsuda N. Vascular endotheliitis associated with infections: its pathogenetic role and therapeutic implication. Biochem Pharmacol. 2022;197: 114909.
7. Yu Q, Wang D, Wen X, Tang X, Qi D, He J, et al. Adipose-derived exosomes protect the pulmonary endothelial barrier in ventilator-induced lung injury by inhibiting the TRPV4/Ca(2+) signaling pathway. Am J Physiol Lung Cell Mol Physiol. 2020;318(4):L723–41.
8. Binnie A, Tsang JLY, Hu P, Carrasqueiro G, Castelo-Branco P, Dos Santos CC. Epigenetics of sepsis. Crit Care Med. 2020;48(5):745–56.
9. Cross D, Drury R, Hill J, Pollard AJ. Epigenetics in sepsis: understanding its role in endothelial dysfunction, immunosuppression, and potential therapeutics. Front Immunol. 2019;10:1363.
10. Li Y. Modern epigenetics methods in biological research. Methods. 2021;187:104–13.
11. Tsagaratou A, Aijo T, Lio CW, Yue X, Huang Y, Jacobsen SE, et al. Dissecting the dynamic changes of 5-hydroxymethylcytosine in T-cell development and differentiation. Proc Natl Acad Sci USA. 2014;111(32):E3306–15.
12. Wu H, Zhang Y. Reversing DNA methylation: mechanisms, genomics, and biological functions. Cell. 2014;156(1–2):45–68.
13. Huang X, Kong G, Li Y, Zhu W, Xu H, Zhang X, et al. Decitabine and 5-azacitidine both alleviate LPS induced ARDS through anti-inflammatory/antioxidant activity and protection of glycocalyx and inhibition of MAPK pathways in mice. Biomed Pharmacother. 2016;84:447–53.
14. Shih CC, Liao MH, Hsiao TS, Hii HP, Shen CH, Chen SJ, et al. Procainamide inhibits dna methylation and alleviates multiple organ dysfunction in rats with endotoxic shock. PLoS ONE. 2016;11(9): e0163690.
15. Singer BD, Mock JR, Aggarwal NR, Garibaldi BT, Sidhaye VK, Florez MA, et al. Regulatory T cell DNA methyltransferase inhibition accelerates resolution of lung inflammation. Am J Respir Cell Mol Biol. 2015;52(5):641–52.
16. Zhang XQ, Lv CJ, Liu XY, Hao D, Qin J, Tian HH, et al. Genome-wide analysis of DNA methylation in rat lungs with lipopolysaccharide-induced acute lung injury. Mol Med Rep. 2013;7(5):1417–24.
17. de la Rica L, Rodríguez-Ubreva J, García M, Islam AB, Urquiza JM, Hernando H, et al. PU.1 target genes undergo Tet2-coupled demethylation and DNMT3b-mediated methylation in monocyte-to-osteoclast differentiation. Genome Biol. 2013;14(9):R99.
18. Wu X, Zhang Y. TET-mediated active DNA demethylation: mechanism, function and beyond. Nat Rev Genet. 2017;18(9):517–34.
19. Delhommeau F, Dupont S, Della Valle V, James C, Trannoy S, Massé A, et al. Mutation in TET2 in myeloid cancers. N Engl J Med. 2009;360(22):2289–301.
20. Bao Y, Bai M, Zhu H, Yuan Y, Wang Y, Zhang Y, et al. DNA demethylase Tet2 suppresses cisplatin-induced acute kidney injury. Cell Death Discov. 2021;7(1):167.
21. Cong B, Zhang Q, Cao X. The function and regulation of TET2 in innate immunity and inflammation. Protein Cell. 2021;12(3):165–73.
22. Cull AH, Snetsinger B, Buckstein R, Wells RA, Rauh MJ. Tet2 restrains inflammatory gene expression in macrophages. Exp Hematol. 2017;55(56–70): e13.
23. Fuster JJ, MacLauchlan S, Zuriaga MA, Polackal MN, Ostriker AC, Chakraborty R, et al. Clonal hematopoiesis associated with TET2 deficiency accelerates atherosclerosis development in mice. Science. 2017;355(6327):842–7.
24. Ma S, Wan X, Deng Z, Shi L, Hao C, Zhou Z, et al. Epigenetic regulator CXXC5 recruits DNA demethylase Tet2 to regulate TLR7/9-elicited IFN response in pDCs. J Exp Med. 2017;214(5):1471–91.
25. Scherm MG, Serr I, Zahm AM, Schug J, Bellusci S, Manfredini R, et al. miRNA142-3p targets Tet2 and impairs Treg differentiation and stability in models of type 1 diabetes. Nat Commun. 2019;10(1):5697.
26. Zhang Q, Zhao K, Shen Q, Han Y, Gu Y, Li X, et al. Tet2 is required to resolve inflammation by recruiting Hdac2 to specifically repress IL-6. Nature. 2015;525(7569):389–93.
27. Qin W, Brands X, Van't Veer C, de Vos AF, Scicluna BP, van der Poll T. Bronchial epithelial Tet2 maintains epithelial integrity during acute *Pseudomonas aeruginosa* pneumonia. Infect Immun. 2020;89(1): e00603.
28. Potus F, Pauciulo MW, Cook EK, Zhu N, Hsieh A, Welch CL, et al. Novel mutations and decreased expression of the epigenetic regulator TET2 in pulmonary arterial hypertension. Circulation. 2020;141(24):1986–2000.
29. Zeng Z, Li T, Liu X, Ma Y, Luo L, Wang Z, et al. DNA dioxygenases TET2 deficiency promotes cigarette smoke induced chronic obstructive pulmonary disease by inducing ferroptosis of lung epithelial cell. Redox Biol. 2023;67: 102916.
30. Hao Y, Fu H, Li K, Zou X, Zhou X, Tang X, et al. Inhibition of GBP1 alleviates pyroptosis of human pulmonary microvascular endothelial cells through STAT1/NLRP3/GSDMD pathway. Mol Immunol. 2024;173:1–9.
31. Xu F, Zhou F. Inhibition of microRNA-92a ameliorates lipopolysaccharide-induced endothelial barrier dysfunction by targeting ITGA5 through the PI3K/Akt signaling pathway in human pulmonary microvascular endothelial cells. Int Immunopharmacol. 2020;78: 106060.

32. Zou X, Liu C, Huang Z, Xiang S, Li K, Yuan Y, et al. Inhibition of STEAP1 ameliorates inflammation and ferroptosis of acute lung injury caused by sepsis in LPS-induced human pulmonary microvascular endothelial cells. Mol Biol Rep. 2023;50(7):5667–74.
33. Rittirsch D, Huber-Lang MS, Flierl MA, Ward PA. Immunodesign of experimental sepsis by cecal ligation and puncture. Nat Protoc. 2009;4(1):31–6.
34. Shi Y, Li B, Huang X, Kou W, Zhai M, Zeng Y, et al. Loss of TET2 impairs endothelial angiogenesis via downregulating STAT3 target genes. Cell Biosci. 2023;13(1):12.
35. Zhang M, Wang J, Zhang K, Lu G, Liu Y, Ren K, et al. Ten-eleven translocation 1 mediated-DNA hydroxymethylation is required for myelination and remyelination in the mouse brain. Nat Commun. 2021;12(1):5091.
36. Han S, Yuan R, Cui Y, He J, Wang QQ, Zhuo Y, et al. Hederasaponin C alleviates lipopolysaccharide-induced acute lung injury in vivo and in vitro through the PIP2/NF-kappaB/NLRP3 signaling pathway. Front Immunol. 2022;13: 846384.
37. Ling X, Wei S, Ling D, Cao S, Chang R, Wang Q, et al. Irf7 regulates the expression of Srg3 and ferroptosis axis aggravated sepsis-induced acute lung injury. Cell Mol Biol Lett. 2023;28(1):91.
38. Bao Y, Wang L, Shi L, Yun F, Liu X, Chen Y, et al. Transcriptome profiling revealed multiple genes and ECM-receptor interaction pathways that may be associated with breast cancer. Cell Mol Biol Lett. 2019;24:38.
39. Quan XJ, Liang CL, Sun MZ, Zhang L, Li XL. Overexpression of steroid receptor coactivators alleviates hyperglycemia-induced endothelial cell injury in rats through activating the PI3K/Akt pathway. Acta Pharmacol Sin. 2019;40(5):648–57.
40. Li H, Shen X, Ma M, Liu W, Yang W, Wang P, et al. ZIP10 drives osteosarcoma proliferation and chemoresistance through ITGA10-mediated activation of the PI3K/AKT pathway. J Exp Clin Cancer Res. 2021;40(1):340.
41. Tong W, Li J, Feng X, Wang C, Xu Y, He C, et al. Kaiso regulates osteoblast differentiation and mineralization via the Itga10/PI3K/AKT signaling pathway. Int J Mol Med. 2021;47(4):41.
42. Tsagaratou A, Lio CJ, Yue X, Rao A. TET methylcytosine oxidases in T cell and B cell development and function. Front Immunol. 2017;8:220.
43. Dejager L, Pinheiro I, Dejonckheere E, Libert C. Cecal ligation and puncture: the gold standard model for polymicrobial sepsis? Trends Microbiol. 2011;19(4):198–208.
44. Qiao X, Yin J, Zheng Z, Li L, Feng X. Endothelial cell dynamics in sepsis-induced acute lung injury and acute respiratory distress syndrome: pathogenesis and therapeutic implications. Cell Commun Signal. 2024;22(1):241.
45. Okashita N, Kumaki Y, Ebi K, Nishi M, Okamoto Y, Nakayama M, et al. PRDM14 promotes active DNA demethylation through the ten-eleven translocation (TET)-mediated base excision repair pathway in embryonic stem cells. Development. 2014;141(2):269–80.
46. Maiti G, Frikeche J, Lam CY, Biswas A, Shinde V, Samanovic M, et al. Matrix lumican endocytosed by immune cells controls receptor ligand trafficking to promote TLR4 and restrict TLR9 in sepsis. Proc Natl Acad Sci USA. 2021. https://doi.org/10.1073/pnas.2100999118.
47. Dayang EZ, Luxen M, Kuiper T, Yan R, Rangarajan S, van Meurs M, et al. Pharmacological inhibition of focal adhesion kinase 1 (FAK1) and anaplastic lymphoma kinase (ALK) identified via kinome profile analysis attenuates lipopolysaccharide-induced endothelial inflammatory activation. Biomed Pharmacother. 2021;133: 111073.
48. Chastney MR, Kaivola J, Leppänen VM, Ivaska J. The role and regulation of integrins in cell migration and invasion. Nat Rev Mol Cell Biol. 2025;26(2):147–67.
49. Wang J, An Z, Wu Z, Zhou W, Sun P, Wu P, et al. Spatial organization of PI3K-PI(3,4,5)P(3)-AKT signaling by focal adhesions. Mol Cell. 2024;84(22):4401-18.e9.
50. Zheng Y, Zhou R, Cai J, Yang N, Wen Z, Zhang Z, et al. Matrix stiffness triggers lipid metabolic cross-talk between tumor and stromal cells to mediate bevacizumab resistance in colorectal cancer liver metastases. Cancer Res. 2023;83(21):3577–92.
51. Shi J, Yu J, Zhang Y, Wu L, Dong S, Wu L, et al. PI3K/Akt pathway-mediated HO-1 induction regulates mitochondrial quality control and attenuates endotoxin-induced acute lung injury. Lab Invest. 2019;99(12):1795–809.
52. Zhang L, Ge S, He W, Chen Q, Xu C, Zeng M. Ghrelin protects against lipopolysaccharide-induced acute respiratory distress syndrome through the PI3K/AKT pathway. J Biol Chem. 2021;297(3): 101111.
53. Wang L, Tang X, Li S. Propofol promotes migration, alleviates inflammation, and apoptosis of lipopolysaccharide-induced human pulmonary microvascular endothelial cells by activating PI3K/AKT signaling pathway via upregulating APOM expression. Drug Dev Res. 2022;83(2):397–406.
54. Gong B, Wang L, Zhang H, Wang Q, Li W. Amplifying T cell-mediated antitumor immune responses in nonsmall cell lung cancer through photodynamic therapy and anti-PD1. Cell Biochem Funct. 2024;42(1): e3925.
55. Goyer B, Theriault M, Gendron SP, Brunette I, Rochette PJ, Proulx S. Extracellular matrix and integrin expression profiles in Fuchs endothelial corneal dystrophy cells and tissue model. Tissue Eng Part A. 2018;24(7–8):607–15.

Publisher's Note